Rare Metal Materials and Engineering
Volume 53, Issue 5, May 2024
Available online at www.rmme.ac.cn

Science Press

Cite this article as: Kang Minglong, Deng Yunlai, Lei Jinqin. Effect of Roughness and Intermetallic Particles on Surface Corrosion of A6111 Alloy[J]. Rare Metal Materials and Engineering, 2024, 53(05): 1252-1261. DOI: 10.12442/j.issn.1002-185X.E20230036.

ARTICLE

Effect of Roughness and Intermetallic Particles on Surface Corrosion of A6111 Alloy

Kang Minglong[1], Deng Yunlai[1,2], Lei Jinqin[3]

[1] Light Alloy Research Institute, Central South University, Changsha 410083, China; [2] Key Laboratory of Nonferrous Materials Science and Engineering, Ministry of Education, Central South University, Changsha 410083, China; [3] Northeast Light Alloy Co., Ltd, Harbin 150060, China

Abstract: Four-layer aluminum brazing sheets (4343/3003/6111/3003) with honeycomb sandwich structure are used as candidates for floor of high-speed train and ship deck, which are often exposed to corrosive environments. Microstructure and surface conditions of optimized 6111 aluminum alloy, which serves as the main support layer of this four-layer brazing sheet, have a great effect on the corrosion properties, which were investigated by a set of 6111 aluminum alloy ground with sandpaper of different grits. The results show that the AlFeSi(Mn, Cu) phase acts as cathode, due to its higher potential than that of the matrix, and forms a multi-stage system with adjacent matrix, which aggravates the surface corrosion. A smoother surface exhibits better corrosion resistance. Specifically, when lowering surface roughness from 18.03 μm to 0.92 μm, the surface volume decreases from 0.629 mm^3 to 0.029 mm^3, and the average number of intermetallic particles AlFeSi (Mn, Cu) is reduced from 1631 mm^{-2} to 917 mm^{-2}, with area fraction decreasing from 3.93% to 0.92%. As a consequence, the average corrosion depth decreases from 237 μm to 95 μm.

Key words: A6111 alloy; surface roughness; intermetallic particles; corrosion resistance; electrochemical test

Aluminum alloy brazing sheet is usually composed of a three-layer structure including two brazing layers (clad layer) and one support layer (core layer). It is widely used in railway, marine and automotive industries due to its low density, high thermal conductivity and excellent brazing performance[1–3]. To reduce mass and cost, it is necessary to reduce the thickness of brazing sheet[4]. However, thin brazing sheet must withstand high temperatures (580–610 °C) during brazing and is prone to collapse[2–3]. Therefore, it is necessary to improve the high-temperature mechanical strength of brazing sheet[3,5].

In order to improve the high-temperature deformation resistance of the brazing sheet, researchers have carried out a large number of studies mainly on optimizing the alloy composition of core layer and improving brazing process, composite manufacturing process, and heat treatment. Zhao et al[6] investigated the effect of annealing process on sagging resistance of 4343/3003/4343 three-layer brazing sheet, and demonstrated that Si diffusion is the main factor affecting the sagging resistance. Lee et al[1–2] investigated the sagging resistance of three-layer brazed composite sheet Al-Si/Al-Mn-Zn/Al-Si, and found that the sagging resistance can be improved by controlling cold rolling rate of reduction and applying intermediate annealing to obtain coarse recrystallized grains. However, most studies focus on the conventional three-layer brazing composite sheet.

To further improve the collapse resistance of brazing composite sheet[7], a new 4343/3003/6111/3003 four-layer aluminum brazing sheet was developed in this research. By optimizing the composition of Mg, Si, Mn and Cu in the 6111 aluminum alloy, which serves as the main supporting layer (core layer), the strength of the four-layer aluminum brazing sheet was increased by 50% compared with that of the conventional three-layer aluminum brazing sheets[8]. The 4343/3003/6111/3003 four-layer aluminum brazing sheets are used as panels for honeycomb sandwich structures, which are employed in applications such as the flooring of high-speed trains and the decks of ships. As the working environment is often contaminated by rain, seawater and salt, the aluminum brazing sheet requires not only higher strength but also higher corrosion resistance. We further optimized 6111 aluminum

Received date: September 16, 2023
Foundation item: National Natural Science Foundation of China (51705539); Major State Research Program of China (2016YFB0300901)
Corresponding author: Deng Yunlai, Ph. D., Professor, Key Laboratory of Nonferrous Materials Science and Engineering, Ministry of Education, Light Alloy Research Institute, Central South University, Changsha 410083, P. R. China, E-mail: 173801016@csu.edu.cn

alloy by adding Cu of high content. These additional Cu atoms help to increase the potential difference between precipitated phase and surrounding matrix, thus affecting corrosion resistance[9–12]. Therefore, studying the corrosion properties of the 6111 aluminum alloy is of paramount importance.

The initial corrosion of aluminum alloys is strongly influenced by the condition of the surface[13–14]. During the machining process, such as cutting, rolling and grinding, the workpiece surface undergoes severe shear plastic deformation. These surface deformations result in uneven distribution of microstructures such as grain boundaries, dislocations, mechanical defects and second phases, which themselves are uniform. This inhomogeneity in the distribution of microstructure will bring about electrochemical inhomogeneity[15–17], and leads to corrosion of the surface. Eckermann et al[18] studied the corrosion process of Al-Mg-Si aluminum alloys and found that the surface layer is different from the bulk materials and the surface deformed layer is more prone to intergranular attack. Due to the abundant defects on the deformed surface, such as impurities, inclusions and ultra-fine crystals, it is easy to cause corrosion sensitivity[15]. Svenningsen et al[19] studied sensitivity of cooling rate to intercrystalline corrosion for Cu-containing 6xxx aluminum alloy after solution heat treatment. They found that cooling rate after solution heat treatment at 540 °C has a major influence on corrosion performance. AlMgSi(Cu) alloy is resistant to intergranular corrosion when quenched rapidly in water. However, little attention has been paid to the effect of intermetallic particle (IMP) distribution on intergranular corrosion.

In this study, the effects of IMPs on intergranular corrosion and electrochemical corrosion of A6111 aluminum alloy with different surface roughnesses were studied by intergranular corrosion test, potentiodynamic polarization tests, open circuit potential (OCP) tests, electrochemical impedance spectroscopy (EIS) test, optical microscope (OM), scanning electron microscope (SEM), atomic force microscope (AFM) and transmission electron microscope (TEM). Average number, average size and average area fraction of the IMPs at different surface roughnesses were analyzed. These studies provide a basis for further improving corrosion resistance of brazing composite sheet.

1 Experiment

1.1 Material and heat treatment

The chemical composition of the as-cast Al-Mg-Si-Cu (A6111) aluminum alloy is presented in Table 1. The casting process was carried out in a crucible resistance furnace at approximately 750 °C, with the feeding order as follows: Al (99 wt%), intermediate alloys (Al-50wt% Cu, Al-10wt% Si and Al-10wt% Mn), Zn (99wt%), Mg (99wt%), Fe (99wt%) and Ti (99wt%). After degassing the melt, the ingot of 30 mm×200 mm×150 mm was cast by steel mold.

Table 1 Chemical compositions of A6111 alloy (wt%)

Mg	Si	Cu	Mn	Fe	Zn	Ti	Al
0.8	1.0	0.9	0.3	<0.27	<0.05	<0.10	Bal.

The cast ingots underwent milling, followed by homogenization at 550 °C for 30 h, and then hot rolled and cold rolled to achieve a thickness of 2 mm. Specimens were cut from the sheets and subjected to solution treatment at 600 °C for 40 min (i.e., the samples were held at 600 °C for 20 min and then the furnace door was opened for cooling to 400 °C), followed by water quenching process. Finally, the samples were aged at 180 °C for 8 h.

Samples of 10 mm×10 mm×2 mm were cut by electric spark cutting machine along the rolling direction. The samples were then ground with 80#, 400#, and 1200# silicon carbide paper and polished at 260 r/min. The exposure area of sample was 10 mm×10 mm. After polishing to the same depth, the samples were unidirectionally ground with 80#, 400#, and 1200# SiC paper and polished, named as 80-grit, 400-grit, 1200-grit and polished. The ground samples were cleaned by deionized water and air-dried.

1.2 Corrosion test

According to the national standard GB/T7998-2005, corrosion solution was prepared by dissolving 20 g NaCl and 66 mL 38% hydrochloric acid in 1 L deionized water. The surface of each sample was exposed and other sides were sealed with rosin and paraffin. The ratio of exposure area to solution volume was maintained at 2.0 dm^2/L, and the temperature was controlled at 35±3 °C. Each group consisted of three parallel samples. After immersion for 24 h, the corroded samples were cut perpendicular to the rolling direction, and the corrosion depth was measured through metallographic examination. The average corrosion depth was calculated from three parallel samples. Additionally, the samples were immersed for 15 and 30 min to observe the exposed surface morphology.

1.3 Electrochemical test

The electrochemical test adopted a three-electrode system with Al-Mg-Si-Cu alloy as the working electrode, platinum sheet (SCE) as the auxiliary electrode and saturated calomel electrode as the reference electrode. 3.5wt% NaCl solution was used as the test solution. The scanning rate used for the polarization curve test was 0.33 mV/s. In OCP conditions, the EIS test was carried out in the frequency range of 0.01–100 000 Hz, and the excitation voltage amplitude was 10 mV. ZSimpWin software was used to fit the data. Test began after 15 s of immersion, and three parallel samples were tested in each state.

1.4 Microstructure examination

The surface morphology of the 80-, 400-, and 1200-grit specimens was observed by OM. Surface roughness (R_a) was measured by a laser scanning confocal microscope (Zeiss Axio LSM700). Additionally, microstructure observation and energy-dispersive X-ray spectroscopy (EDS) analysis of the samples were conducted by SEM (ZEISS-EVOM10) at an accelerating voltage of 20 kV. The precipitated phase was characterized by TEM (TecnaiG220) with an acceleration

voltage of 200 kV. The prepared samples had a thickness of 80 μm and a diameter of 3 mm. Electropolishing was conducted in a solution containing 30vol% nitric acid and 70vol% methanol in liquid nitrogen at temperatures ranging from –35 °C to –20 °C.

Scanning Kelvin probe AFM (SKPFM) was used to determine the Volta potential of the alloy surface. Si probe covered with CoCr coating was employed as a reference electrode. Surface morphology and the surface Volta potential were measured by Dimension FastScan AFM. The tests were conducted in an atmospheric environment at a scanning rate of 0.5 Hz. NanoScope Analysis 1.8 software was used to analyze the experimental data.

2 Results

2.1 Surface morphology and roughness

Surface morphologies of 80-grit, 400-grit, 1200-grit and polished samples are shown in Fig.1. The samples are ground with SiC paper with deep scratches along grinding direction. Roughness is regularly arranged on sample surface (as shown in Fig. 1a – 1c). Note that wear traces of 80-grit sample are relatively deeper and narrower than that of 1200-grit sample.

Grooves on the surface are created by the cutting of abrasive particles which are closely related to grit size (grit number). To quantify the surface morphology, surface roughness and corresponding profile, samples were ground with SiC emery paper of different grits. Each roughness curve obtained along the red line reveals three-dimensional surface morphology of the sample, showing the height distribution of the groove. The surface roughness of the samples varies significantly with grit numbers of SiC emery paper. After grinding with 80-grit sandpaper, obvious ridge and parallel valley appear along the scratch direction, and the average depth and width are 56.15 and 25.93 μm, respectively. As the grit size of sandpaper increases from 80 to 1200, the wear marks become shallower and surfaces of the samples become smoother (as shown in Fig. 2c and 2e). No obvious grinding marks are observed for polished samples (Fig.2g). As grit size of sandpaper increases from 80 to 1200, the surface roughness (R_a) decreases from 18.03 μm to 6.12 μm, and thus the surface volume decreases from 0.629 mm^3 to 0.029 mm^3. The surface roughness of the polished sample is the lowest (0.915 μm).

2.2 Coarse IMPs

For different grinding surfaces per square millimeter on the

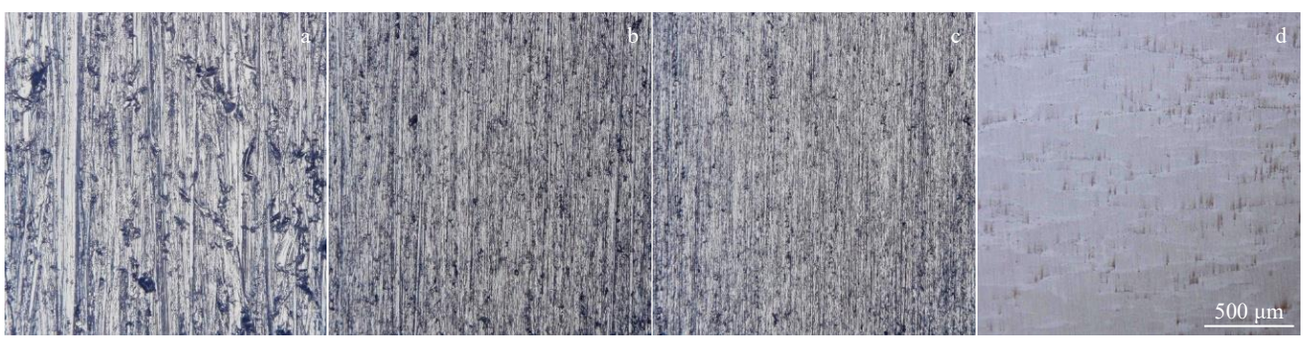

Fig.1 Surface morphologies of 80-grit (a), 400-grit (b), 1200-grit (c), and polished (d) samples

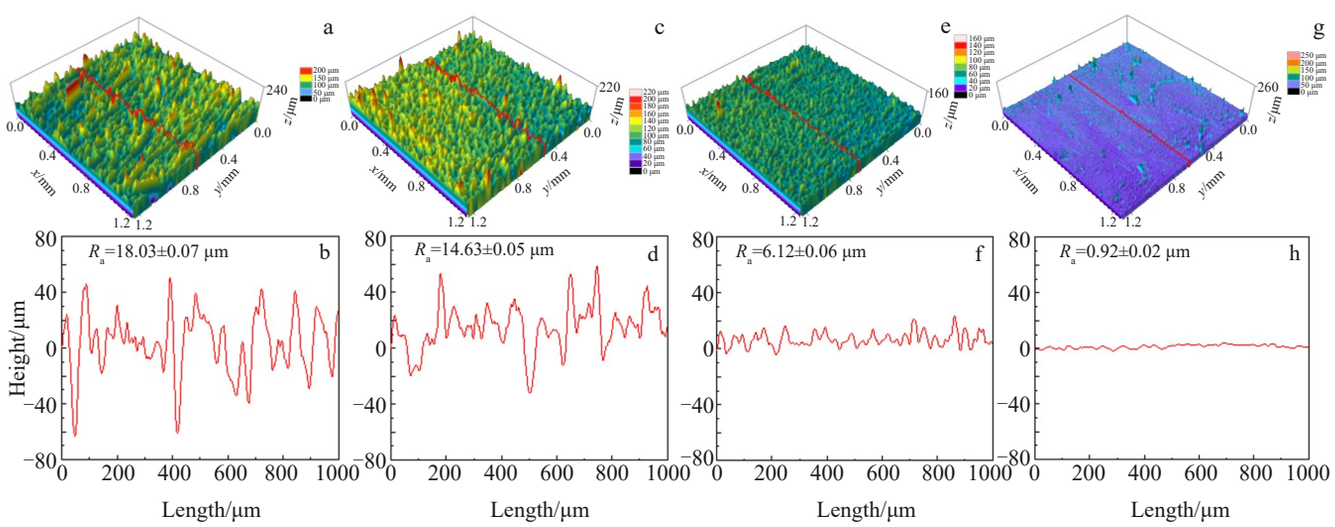

Fig.2 3D surface topographies (a, c, e, g) and profile curves (b, d, f, h) of A6111 alloys: (a – b) 80-grit, (c – d) 400-grit, (e – f)1200-grit, and (g–h) polished

surface, 20× low-magnification, 10× middle-magnification and 10× high-magnification SEM images are used to analyze the size and density of the IMPs, as shown in Fig.3. The white particle is determined to be a composite phase rich in Al, Fe, Si, Mn and Cu by EDS mappings in Fig. 3e. According to TEM image and selected area electron diffraction (SAED) pattern of the phase (Fig.3f and 3g), it can be inferred that the white particle is AlFeSi(Mn, Cu) phase. Large and irregular IMPs are commonly formed during solidification without dissolution in subsequent heat treatment, which are broken and have banded distribution in the machining process. One can see that there is no cavity between the particles and surrounding matrix, which means that the IMPs are not corroded and pulled out during the grinding process.

Fig. 4 shows the size distribution histograms of AlFeSi(Mn,Cu) phases, and the statistical data are list in Table 2. As the grit size increases, the average particle size of AlFeSi(Mn, Cu) IMPs changes slightly, and the area fraction and particle density show a downward trend. During surface grinding, stress and strain decrease with increasing the distance from the surface. Stress and strain are greater in the near-surface layer. Under the action of stress, partial IMPs are

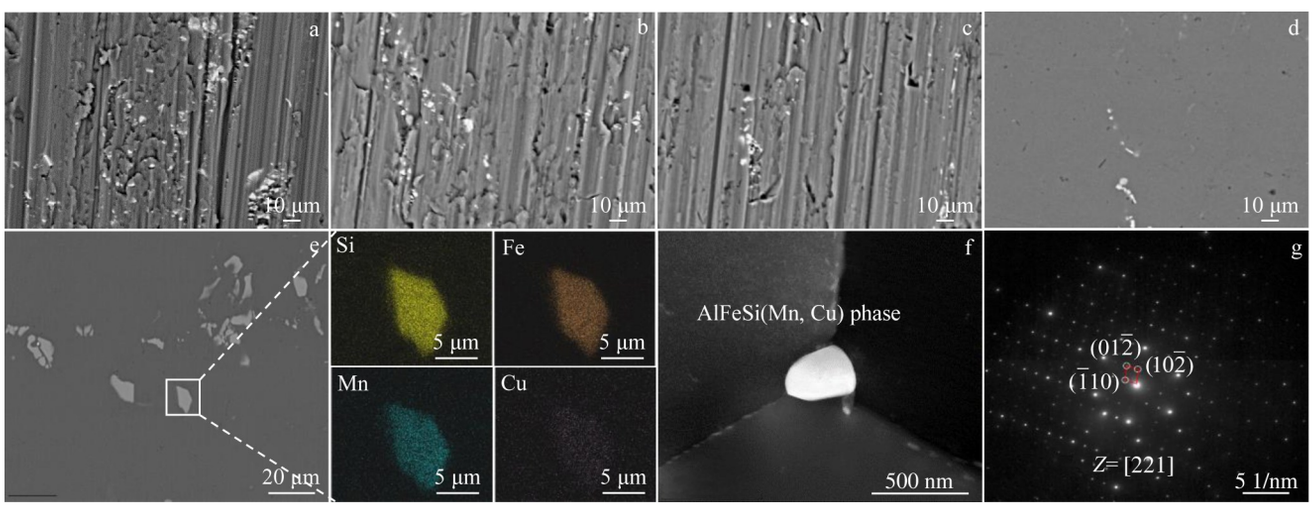

Fig.3 SEM images of Al-Mg-Si-Cu alloys: (a) 80-grit, (b) 400-grit , (c) 1200-grit, and (d) polished; SEM image and EDS results (e); TEM bright field image (f) and corresponding SAED pattern (g) of AlFeSi(Mn, Cu) phase

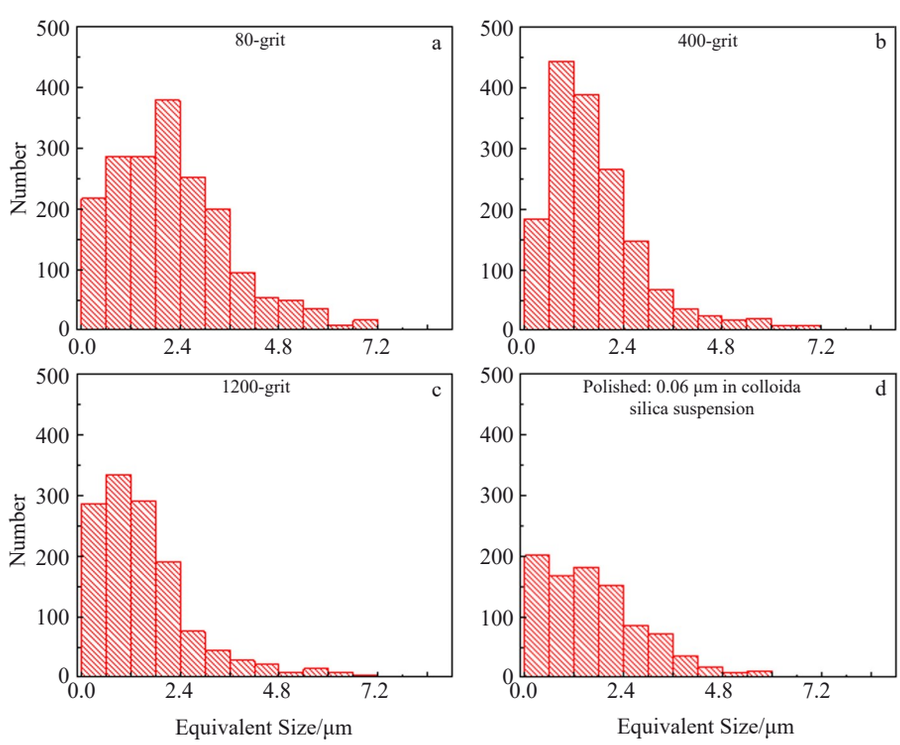

Fig.4 Size distribution histograms of AlFeSi(Mn, Cu) IMPs in Al-Mg-Si-Cu alloys: (a) 80-grit, (b) 400-grit, (c) 1200-grit, and (d) polished

Table 2 Analytical data of AlFeSi(Mn, Cu) IMPs in A6111 alloy

Parameter	80-grit	400-grit	1200-grit	Polished
Particle density/mm^{-2}	1631	1553	1153	917
Average size/μm	2.03	1.63	1.28	0.91
Area fraction/%	3.93	2.12	1.21	0.92

mechanically crushed on the near-surface of A6111 alloy[14]. The surface state (AlFeSi(Mn, Cu) and roughness) is altered by grinding without changing the heat treatment and deformation. Grinding with different grits of sandpaper gives rise to surface roughness, and the surface area of the grinding surface changes accordingly. The larger the grit number of sandpaper, the smaller the resulting roughness, and the actual surface area of the ground surface decreases too, resulting in a decrease in the area fraction of the AlFeSi(Mn, Cu) phase exposed on the surface[20–21]. In addition, grinding will cause change in the cross-sectional area of the exposed AlFeSi(Mn, Cu) phase, and the cross-sectional area of the exposed AlFeSi(Mn, Cu) phase exposed by grinding with different grits of sandpaper will be different, resulting in difference in size.

2.3 Surface Volta potential

SKPFM technique is widely used to study local corrosion behavior of aluminum alloy[22–25]. The corrosion behavior of phase precipitated in A6111 alloy can be further studied by measuring surface Volta potential. Fig. 5 shows the AFM morphologies and Volta potential distribution of regions marked by the white box in Fig. 3e. As seen from Volta potential distribution, AlFeSi(Mn, Cu) phase and the surrounding ma-trix show higher potential. Volta potential changes in Fig.5c show significant difference between AlFeSi (Mn, Cu) and the matrix. According to above results, it can be concluded that there is potential difference between AlFeSi (Mn, Cu) phase and the matrix. The AlFeSi(Mn, Cu) phase has a higher potential than the matrix.

2.4 Localized corrosion behavior

2.4.1 Electrochemical performance

The OCP curves of A6111 alloys treated with four surface finishes are depicted in Fig.6a. Each potential reaches a stable state after a short duration. The OCP values of 80-grit, 400-grit, 1200-grit and polished A6111 alloy samples are −788.4, −768.3, −731.8 and −712.8 mV$_{SCE}$, respectively. It is evident that the OCP moves in the positive direction as the grit number increases. This indicates that smoother surfaces are less active than rougher ones.

Fig. 6b presents the potentiodynamic polarization curves of samples. The corrosion potential (E_{corr}) and corrosion current density (I_{corr}) obtained from the potentiodynamic polarization curves of A6111 alloy treated with four distinct surface finishes are listed in Table 3, utilizing Tafel extrapolation[26–27]. The corrosion behavior of these four samples is analogous, undergoing continuous corrosion processes without passivation. Corrosion potential and corrosion current are commonly used to assess the corrosion resistance of Al alloy, and more positive corrosion potential indicates lower corrosion tendency. Meanwhile, corrosion current serves as a kinetic parameter, higher values of which signify elevated corrosion rates[28]. With the increase in grit number of sandpaper from 80 to 1200, the E_{corr} of the samples gradually moves to the positive direction from −791 mV$_{SCE}$ to −742 mV$_{SCE}$, and the E_{corr} of the polished sample is −730 mV$_{SCE}$. This indicates that the smoother surface of A6111 alloy has lower corrosion sensitivity than the rougher one. According to Faraday's second law, I_{corr} is positively related to the corrosion rate. The corrosion current density of the surface ground with 80-grit sandpaper is 28.8 μA·cm^{-2}. The value for the polished sample, however, is only 1.0 μA·cm^{-2}, indicating that I_{corr} decreases gradually with the decrease in surface roughness, and thus the corrosion resistance is enhanced.

Fig. 6c – 6d depict the impedance spectra and equivalent circuit of the four test samples, respectively. The Nyquist curves of these four samples with different roughnesses consist of low-frequency capacitive reactance arcs and medium-high frequency capacitive reactance arcs. To quantitatively assess the corrosion of A6111 alloy with varying surface roughnesses, the electrochemical parameters of each sample are calculated by ZSimpWin software. In Fig. 6d, R_{ct} represents charge transfer resistance, and a higher R_{ct} value indicates improved corrosion resistance[29–30]. Successively, the arc-reactance radii for the 80-grit, 400-grit and 1200-grit samples are observed to increase, R_{ct} increases

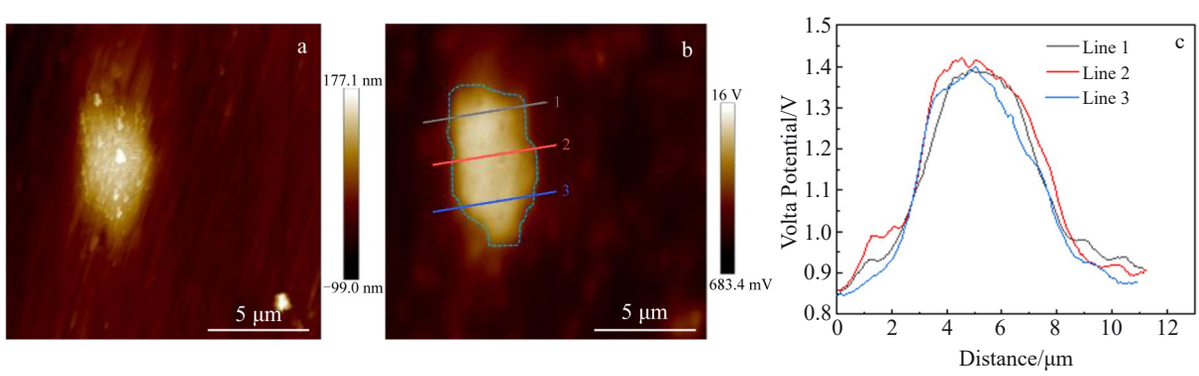

Fig.5 AFM surface topography(a), Volta potential distribution of region marked in Fig. 3e (b), and Volta potential variation curves along lines 1–3 marked in Fig.5b (c)

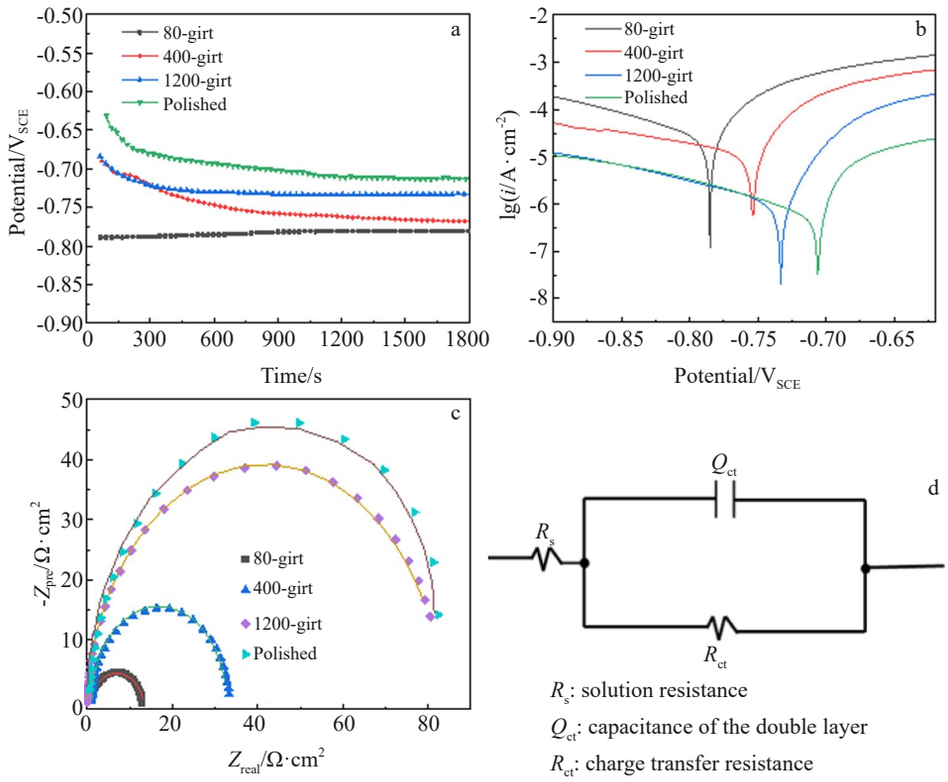

Fig. 6 OCP curves of A6111 alloy with four surface finishes in 3.5wt% NaCl solution (a), correspongding potentiodynamic polarization curves (b), Nyquist plots (c), and equivalent circuit (d) for EIS analysis

Table 3 Electrochemical parameters obtained from the potentiodynamic polarization curves of A6111 alloy with four different surface finishes

Specimen	E_{corr}/mV$_{SCE}$	I_{corr}/μA·cm^{-2}
80-grit	–791±15.0	28.8±1.4
400-grit	–755±11.3	12.3±1.1
1200-grit	–742±13.1	1.1±0.2
Polished	–730±9.8	1.0±0.2

from 12.6 Ω·cm^2 to approximately 31.5 Ω·cm^2, and that of polished sample is up to 83.4 Ω·cm^2. This signifies that the impedance varies, and the surface impedance rises with decreasing the roughness. The four samples exhibit similar impedance characteristics, suggesting comparable corrosion processes. Among the tested samples, the capacitive arc radius of the polished sample is the largest, indicating that the polished sample possesses the best corrosion resistance[31].

2.4.2 Corrosion morphology

Samples after surface corrosion were cut off along transverse direction. The cross-section corrosion morphologies and their average corrosion depth are shown in Fig. 7. When the surface is ground with 80# sandpaper, the maximum corrosion depth is 240 μm. Compared with that of other three samples, the average corrosion depth of 80-grit sample is the largest. Corrosion extends from grain boundary to grain interior seriously. Many black corrosion ditches and corrosion pits penetrate into the microstructure. The entire surface shows serious corrosion and many grains peel off. As grit number of sandpaper increases from 80 to 1200, surface roughness becomes smaller and smaller (average depth of corrosion becomes smaller too), so does the extent of intergranular corrosion. The expansion of corrosion from grain boundary to grain interior decreases gradually. For polished sample, its roughness is the minimum, and corrosion range and corrosion degree are also the smallest with slight expansion of corrosion to grain boundaries, of which the maximum corrosion depth is only 97 μm.

The extent of corrosion can be evaluated by examining the exposed surface, which provides valuable insights for corrosion analysis[32]. Fig. 8 shows the SEM images of corroded surface for polished samples after immersion in the corrosion solution for 15 min. As depicted in Fig. 8a and 8b, numerous pits with diameters ranging from 5 μm to 20 μm are observed. Fig. 8c presents a magnified image of the white box marked in Fig. 8b and EDS line scanning results, which illustrates the changes in Al and Cu element contents of the intergranular phases indicated by the red arrow during the initial corrosion phase. It can be inferred that after the selective dissolution of Al, Fe and other elements, the composition AlFeSi(Mn, Cu) undergoes a transformation, resulting in the formation of a Cu-rich residue. The enrichment of copper amplifies the galvanic corrosion effect between the residue and the neighboring matrix, thereby promoting the continuous expansion of pits and inducing intergranular corrosion (IGC).

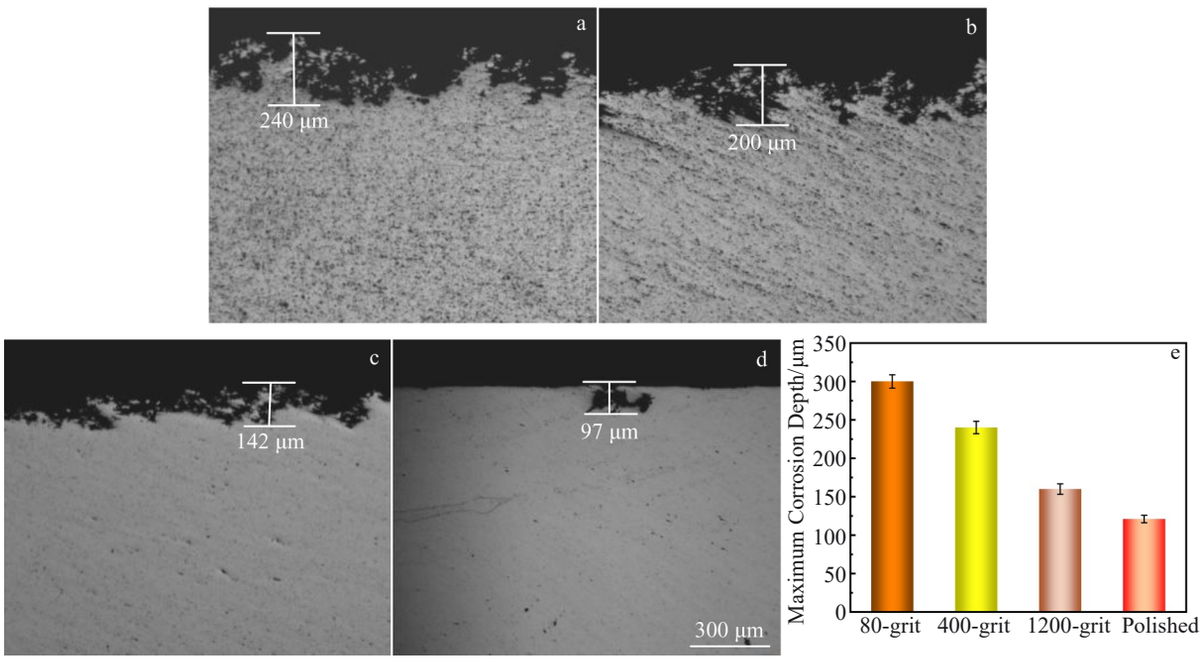

Fig.7 Corrosion morphologies (a–d) and maximum corrosion depth (e) of the four samples after immersion in corrosive solution for 30 min: (a) 80-grit, (b) 400-grit , (c) 1200-grit, and (d) polished

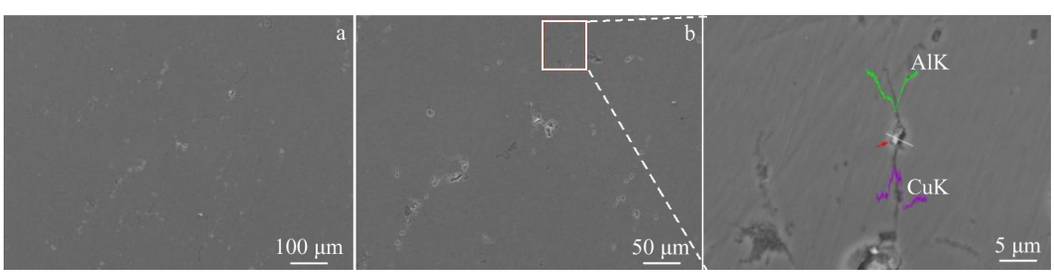

c

Element	wt%	at%
Al	77.2	0.32
Mg	0.4	0.06
Si	2.55	0.09
Mn	1.89	0.13
Fe	3.65	0.17
Cu	14.30	0.23

Fig.8 SEM images of the corroded surface of the polished sample immersed in corrosion solution for 15 min and corresponding EDS results of the intergranular phase marked by red arrow in Fig.8c

Fig. 9 illustrates the exposed surfaces of samples subjected to various grinding conditions and immersed in a corrosive solution for 30 min. It is evident that the surfaces of the four samples exhibit different degrees of attack. The 80-grit sample (Fig. 9a) and the 400-grit sample (Fig. 9b) display severe localized pitting and IGC. As the grit number increases, the severity of localized corrosion decreases. Consequently, the 1200-grit sample (Fig. 9c) and the polished sample (Fig. 9d) exhibit slight localized pitting and IGC on the surface. Based on the analysis of Fig. 7 and Fig. 9, the order of corrosion severity for the four surface conditions in the corrosive solution is as follows: 80-grit>40-grit>1200-grit>polished.

3 Discussion

Corrosion behavior of aluminum and aluminum alloy are closely associated with IMPs, grain boundary precipitation, grain size and non-precipitation zone. The electrochemical inhomogeneity of metal matrix caused by IMPs leads to the preferential dissolution of IMPs and/or surrounding matrix[33–36].

As observed in Fig. 10, the surface roughness R_a decreases from 18.03 μm to 0.92 μm as the processing changes from 80-grit grinding to polishing, and the average size of the AlFeSi(Mn, Cu) phase varies from 2.03 μm to 1.91 μm. Correspondingly, the average number of IMPs AlFeSi(Mn, Cu) is reduced from 1631 μm^{-2} to 917 μm^{-2}, and the area fraction of the AlFeSi(Mn, Cu) phase decreases from 3.93% to 0.92%. Additionally, the surface volume decreases from 0.629 mm^3 to 0.029 mm^3. The rougher surface after grinding corresponds to a larger actual surface area. Therefore, compared with smooth surface, more AlFeSi(Mn, Cu) IMPs are exposed, the area fraction of AlFeSi(Mn, Cu) particles in contact with the surface corrosion solution increases. The corrosion current density concurrently rises with the expansion in actual surface area exposed to the corrosive solution.

As shown in Fig. 11a and 11b, the high-angle annular dark field scanning transmission electron microscopy (HAADF-STEM) images and corresponding EDS line scanning of grain boundaries of A6111 alloy are illustrated. Fig. 11c and 11d are high resolution TEM (HRTEM) image and corresponding fast

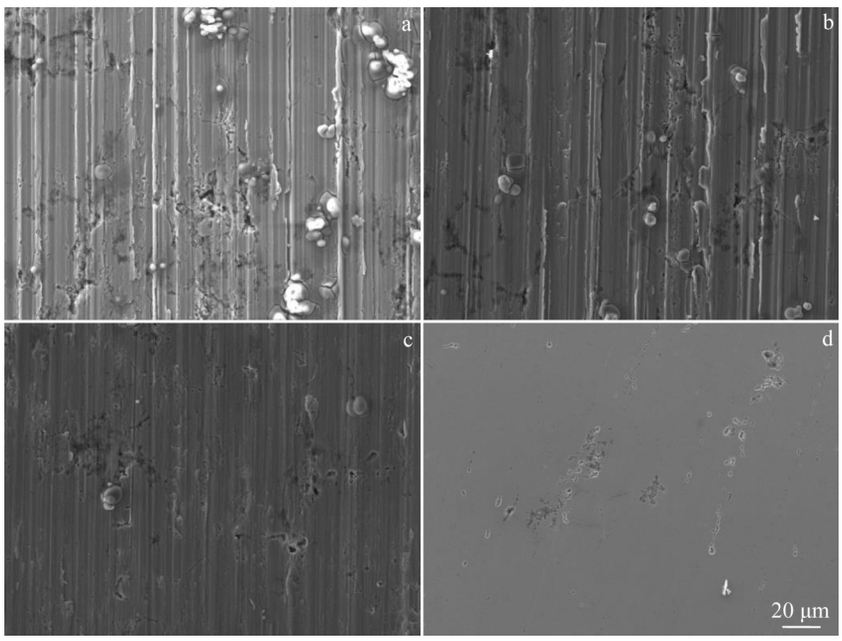

Fig.9 SEM images of surface morphology of samples with different surface states immersed in corrosion solution for 30 min: (a) 80-grit, (b) 400-grit, (c)1200-grit, and (d) polished

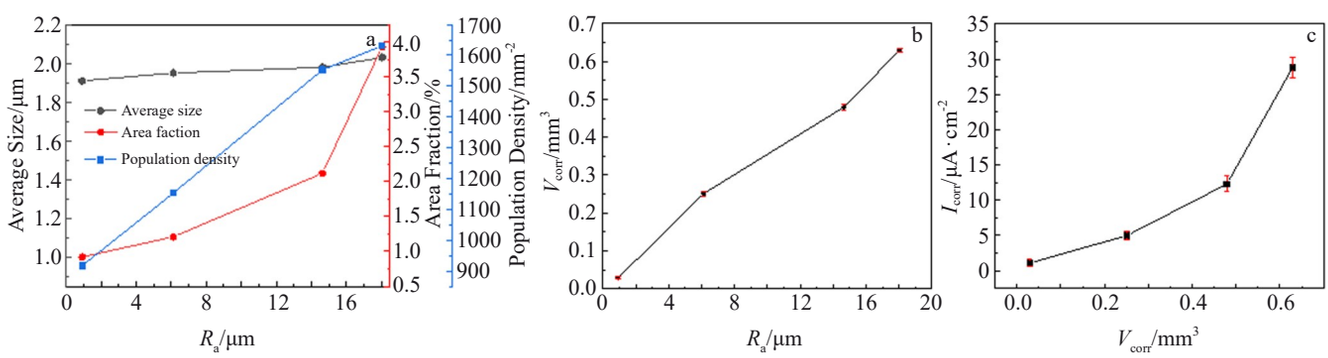

Fig.10 Average size, area fraction and population density as a function of R_a for AlFeSi(Mn, Cu) (a); relationship between R_a and corrosion solution volume V_{corr} (b); relationship between V_{corr} and corrosion current density I_{corr} (c)

Fourier filtering transform (FFT) pattern of the precipitate within red circle in Fig. 11a, respectively. The Q′ phase exhibits a hexagonal crystal structure, characterized by a habit plane of {510}. The unit cell parameters are a=1.032 nm and c =0.405 nm. The precipitate can be identified as the Q′ phase[37]. Based on the EDS line scanning analysis, it can be inferred that the Q′ phase nucleates on AlFeSi(Mn, Cu) IMPs. The low-magnification bright field and dark field images in Fig. 11e and 11f clearly show the distributed AlFeSi(Mn, Cu) phase (marked by red arrows) and Q′ phase (marked by yellow arrows) at the grain boundaries. The Volta potential of IMPs AlFeSi(Mn, Cu) is significantly higher than that of the matrix, and AlFeSi(Mn, Cu) is utilized as the cathode phase. This difference in electrochemical behavior makes the Al alloy sensitive to localized corrosion attacks. Grain boundaries may be susceptible to preferential corrosion attack. AlFeSi(Mn, Cu) particles can be highly active in the galvanic coupling between IMPs and grains, which provides a driving force for the occurrence and expansion of corrosion. This is the cause of corrosion attack[38–39]. With decreasing the sandpaper grit number, both the roughness and the area fraction of the AlFeSi(Mn, Cu) IMP phase increase. The actual surface area of the solution in contact with the alloy surface also increases, leading to more pronounced galvanic corrosion. A relatively larger area fraction of AlFeSi(Mn, Cu) particles means that there are more nucleation sites for the Q′ phase. AlFeSi(Mn, Cu) and Q′ phases, as cathodes, form a multi-stage electrode system with the adjacent matrix region, resulting in poor IGC resistance. The potentiodynamic polarization curve is mainly manifested as the active dissolution area, and the dissolution is controlled by the cathode activity of IMPs. Therefore, the microstructure of surface grinding (mainly AlFeSi(Mn, Cu) phase) significantly influences the IGC of A6111 alloy.

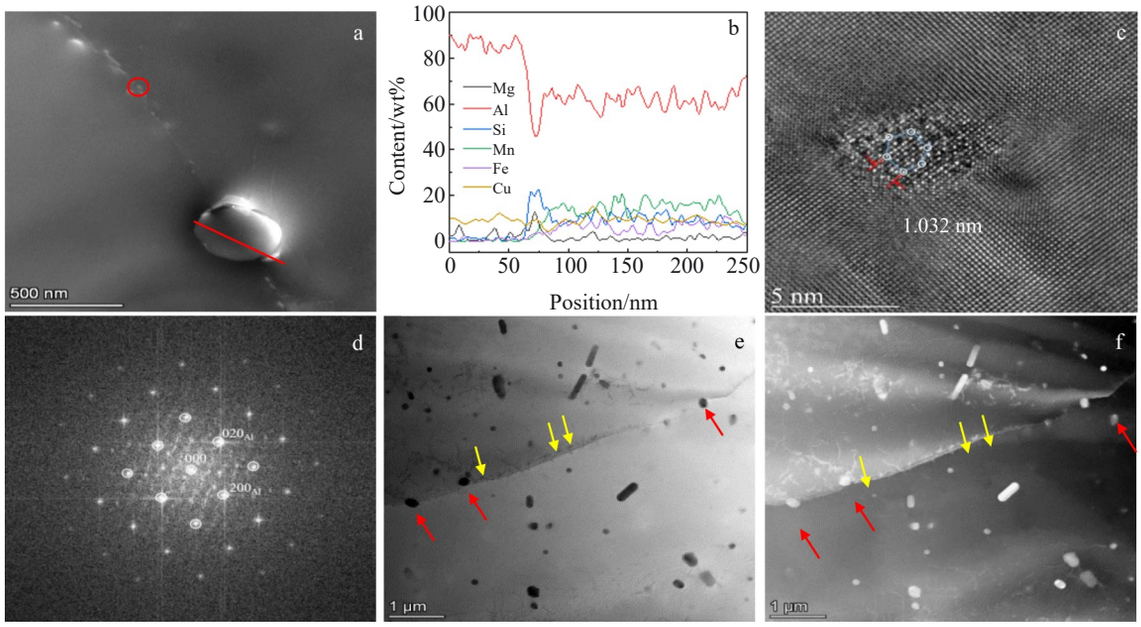

Fig.11 HAADF-STEM image (a) and corresponding EDS line scanning results along the red line of grain boundaries marked in Fig. 11a (b). HRTEM image (c) and corresponding FFT pattern (d) of Q′ phase within the red circle in Fig. 11a; bright field (e) and dark-field (f) images of grain boundary region

In addition, surface fluctuations of metals can cause differences in electrochemical activity. The corrosion reaction rate of metal surfaces increases with the increase in surface roughness. The reason is that the peak position of the sample surface can provide higher electrochemical activity than the valley position, and the surface electrons are easier to react with the environmental medium[40]. According to Fick's first law of diffusion, diffusion process of corrosion to produce water-soluble ions Al^{3+} is related to the diffusion rate. The equation is shown in Eq.(1).

$$\frac{dn}{dc} = -DA\frac{dC}{dx} \quad (1)$$

where dn/dc is material diffusion rate, D is diffusion coefficient, A is diffusion channel surface area, and dC/dx is concentration gradient.

In the same reaction system, the diffusion coefficient D is the same, so the diffusion rate of Al^{3+} is related to the surface area A and the concentration gradient dC/dx. When the sample surface roughness increases, the surface curve of the sample is more undulating and the wave peak is sharper. The concentration gradient is higher, and the radius of curvature is larger, thus making the surface area of diffusion channel A larger. Therefore, the accumulation of corrosion product Al(OH) at the wave peak is reduced and the reaction rate at the wave peak increases.

4 Conclusions

1) Grinding not only changes the surface roughness R_a, but also changes the area fraction of AlFeSi(Mn, Cu) IMPs. From 80-grit grinding to polishing state, the surface roughness R_a for Al-Mg-Si-Cu alloy is decreased from 18.03 μm to 0.92 μm per square millimeter of abraded surface, the average number of IMPs AlFeSi(Mn, Cu) is reduced from 1631 μm^{-2} to 917 μm^{-2}, the area fraction decreases from 3.93% to 0.92%, and the average size of phases changes little.

2) The corrosion potential is significantly different between AlFeSi(Mn, Cu) and matrix. AlFeSi(Mn, Cu) IMPs can be the nucleation sites for Q′ phase. AlFeSi(Mn, Cu) and Q′ phases act as cathodes, which increases the galvanic corrosion effect on adjacent matrix region, resulting in intergranular corrosion.

3) A smoother surface displays lower surface corrosion susceptibility. The lower density and the less area fraction of IMPs on the smoother surface retard surface corrosion. As the grit number increases from 80 to 1200, the corrosion potential increases from −791 mV_{SCE} to −742 mV_{SCE}, the charge transfer resistance increases from 12.6 $\Omega \cdot cm^2$ to 31.5 $\Omega \cdot cm^2$, and the corrosion current density decreases from 28.8 $\mu A \cdot cm^{-2}$ to 5.0 $\mu A \cdot cm^{-2}$; the corresponding values for polished surface are −730 mV_{SCE}, 83.4 $\Omega \cdot cm^2$ and 1.1 $\mu A \cdot cm^{-2}$, respectively.

References

1 Lee S H, Yoon J S, Kim M S *et al. Metals and Materials International A*[J], 2002, 8: 227

2 Lee S H, Kim M S, Jung D *et al. Materials Science Forum*[J], 2003, 439: 221

3 Yoon J S, Lee S H, Kim M S. *Journal of Materials Science Letters*[J], 2001, 20: 229

4 Tu Y, Tong Z, Jiang J. *Metallurgical and Materials Transactions A*[J], 2013, 44: 1760

5 Yoon J S, Lee S H, Kim M S, *Journal of Materials Processing Technology*[J], 2001, 111: 85

6 Zhao Y, Zhang Z, Jin L *et al. Transactions of the Nonferrous*

Metals Society of China[J], 2016, 26: 2542
7 Kimberley W. *Review of Automotive Engineering*[J], 2004, 29: 30
8 Kang M, Zhou L, Deng Y *et al. Metals*[J], 2022, 12(5): 777
9 He L Z, Chen Y B, Cui J Z *et al*. *Corrosion Science and Technology Protection*[J], 2004, 16: 129
10 Zhan H, Mol J M C, Hannour F *et al. Materials and Corrosion*[J], 2008, 59: 670
11 Yamaguchi K, Tohma K. *Journal of Japan Institute of Light Metals*[J], 1997, 47: 285
12 Zou Y, Liu Q, Jia Z H *et al. Applied Surface Science*[J], 2017, 405: 489
13 Wang S S, Yang F, Frankel G S. *Journal of the Electrochemical Society*[J], 2017, 164: C317
14 Zhou X, Liu Y, Thompson G E *et al. Metallurgical and Materials Transactions A*[J], 2011, 42: 1373
15 Afseth A, Nordlien J H, Scamans G M. *Corrosion Science*[J], 2001, 43(12): 2359
16 Wang S, Jiang J, Fan G *et al*. *Materials Characterization*[J], 2014, 98: 18
17 Liu B, Zhang X, Zhou X *et al*. *Corrosion Science*[J], 2017, 126: 265
18 Eckermann F, Suter T, Uggowitzer P J *et al. Corrosion Science*[J], 2008, 50(12): 3455
19 Svenningsen G, Larsen M H, Nordlien J H *et al*. *Corrosion Science*[J], 2006, 48(1): 258
20 Chi G, Yi D, Liu H. *Journal of Materials Research and Technology*[J], 2020, 9: 1162
21 Liu J, Zhao K, Yu M *et al. Corrosion Science*[J], 2018, 138: 75
22 Song F X, Zhang X M, Liu S D *et al. Corrosion Science*[J], 2014, 78: 276
23 Ly R, Hartwig K T, Castaneda H. *Materialia*[J], 2018, 4: 457
24 Sun Y W, Pan Q L, Sun Y Q *et al. Journal of Alloys and Compounds*[J], 2019, 783: 329
25 Schmutz P, Frankel G S. *Journal of the Electrochemical Society*[J], 1998, 145: 2285
26 Chakrabarti D J, Laughlin D E. *Progress in Materials Science*[J], 2004, 49: 389
27 Svenningsen G, Lein J E, Bjørgum A *et al. Corrosion Science*[J], 2006, 48(1): 226
28 Zuo J R, Hou L G, Shi J T *et al. Journal of Alloys and Compounds*[J], 2017, 716: 220
29 Liu S D, Chen B, Li C B *et al. Corrosion Science*[J], 2015, 91: 203
30 Keddam M, Kuntz C, Takenouti H *et al. Electrochimica Acta*[J], 1997, 42: 87
31 Cui X M, Cui H, Zhao X P *et al. Rare Metal Materials and Engineering*[J], 2023, 52(9): 3179
32 Lin Y C, Zhang J L, Liu G *et al. Materials and Design*[J], 2015, 83: 866
33 Ma Y, Zhou X, Huang W *et al. Materials Chemistry and Physics*[J], 2015, 161: 201
34 Zhang Peng, Zhao Xinsheng, Rao Sixian. *Rare Metal Materials and Engineering*[J], 2023, 52(5): 1573
35 Olugbade T O. *Metals and Materials International*[J], 2023, 29(9): 2415
36 E Shun, Deng Jiacheng, Wang Henan *et al. Rare Metal Materials and Engineering*[J], 2023, 52(6): 2048 (in Chinese)
37 Torsæter M, Lefebvre W, Marioara C D *et al. Scripta Materialia*[J], 2011, 64: 817
38 Zhu Huixin, Huang Zhiyong, Jin Guofeng *et al. Rare Metal Materials and Engineering*[J], 2022, 51(8): 3103 (in Chinese)
39 Vargel C. *Corrosion of Aluminium*[M]. Oxford: Elsevier, 2004
40 Li W, Li D. *Acta Materialia*[J], 2006, 54: 445

粗糙度和金属间化合物粒子对A6111铝合金表面腐蚀的影响

康明龙[1]，邓运来[1,2]，雷金琴[3]
(1. 中南大学 轻合金研究院，湖南 长沙 410083)
(2. 中南大学 有色金属材料科学与工程教育部重点实验室，湖南 长沙 410083)
(3. 东北轻合金有限责任公司，黑龙江 哈尔滨 150060)

摘 要：钎焊铝蜂窝夹层结构板常用于高速列车的地板和船舶的甲板。其中四层铝复合板（4343/3003/6111/3003）作为该蜂窝结构的面板常暴露于腐蚀性环境中。经过成分优化的6111铝合金作为四层铝复合板的主要支撑层材料，其组织结构和表面状态对腐蚀 性能有很大影响。采用不同粒度的砂纸磨削6111铝合金，研究了不同程度磨削后6111铝合金的微观组织和表面腐蚀行为。结果表明：6111合金中的AlFeSi(Mn, Cu)相的电位高于基体电位，这种相作为阴极与相邻基体形成多级体系，加剧了表面腐蚀。同时，较光滑的表面具有更好的耐腐蚀性。当表面粗糙度从18.03 μm降至0.92 μm时，表面几何体积由0.629 mm^3减少至0.029 mm^3，金属间化合物AlFeSi(Mn，Cu)粒子的平均数量由1631 mm^{-2}减少至917 mm^{-2}，其面积分数由3.93%降至0.92%。相应地，平均腐蚀深度由237 μm降至95 μm。

关键词：6111铝合金；表面粗糙度；金属间化合物颗粒；耐腐蚀性；电化学测试

作者简介：康明龙，男，1980年生，博士，讲师，中南大学轻合金研究院，湖南 长沙 410083，E-mail：173801016@csu.edu.cn